MDPI

Article

Mitigating Effect of Urban Green Spaces on Surface Urban Heat Island during Summer Period on an Example of a Medium Size Town of Zvolen, Slovakia

Veronika Murtinová, Igor Gallay and Branislav Olah *

Department of Applied Ecology, Faculty of Ecology and Environmental Sciences, Technical University in Zvolen, T.G. Masaryka 24, SK-960 01 Zvolen, Slovakia
* Correspondence: olah@tuzvo.sk; Tel.: +421-45-5206-506

Abstract: Climate change affects the urban population's health and quality of life. Urban green spaces (UGS) underpin several essential ecosystem services, amongst them climate regulation. Urban vegetation mitigates high temperatures and, thus, reduces the heat stress for urban residents. The study aimed to verify whether the Surface Urban Heat Island (SUHI) effect manifests itself even in a medium size town (Zvolen, Slovakia) surrounded by agricultural and forested landscape and to quantify the temperature mitigating effect of urban green spaces. Land surface temperature (LST) and SUHI distribution were derived from the Landsat data during the summer months of 2010–2021. To statistically prove the cooling effect of the urban vegetation, we tested (by one-way ANOVA) LST within three urban zones of the Zvolen municipality defined by the Copernicus imperviousness density data: (a) dense urban area (31–100% impervious surfaces), (b) discontinuous urban area (1–30% impervious surfaces), (c) urban green spaces (0% impervious surfaces), and the open land surrounding the town (0% impervious surfaces). The results showed a statistical difference in temperatures between all urban areas (all zones) and the open land. Moreover, the UGS temperature was statistically different compared to the other urban zones. The mean temperature difference through the years 2010–2021 between urban green spaces and the dense urban area was 3.5 °C, with a maximum of 4.9 °C and a minimum 1.7 °C in favor of the urban spaces. Moreover, the temperature of urban green spaces and open land varied during the studied summer period. The warmer the weather, the higher the difference, while at the end of August, on a notably colder day, there was no significant difference between them. The results confirmed that UGS are significantly cooler during hot days, and they can mitigate the local climate.

Keywords: surface urban heat island; urban green spaces; land surface temperature; climate mitigation; Landsat

1. Introduction

According to the United Nations, the expanding urban population accounted for 55% in 2018, is expected to rise to 68% by 2050 [1]. One of the many consequences of urbanization is the expansion of cities into rural areas, which leads to the transformation of lands from natural surfaces to developed surfaces, and to an increase in impervious surfaces, such as stone, concrete, asphalt, metal, and other materials with a tendency to trap heat and overheat, that release heat more quickly [2,3]. The condition of urban ecosystems affects human well-being [4] and how cities impact their surroundings [5]. As a result, significant changes in the urban climate can occur [6–8]. Research has shown that cities are almost always warmer than their surroundings. This phenomenon is known as the urban heat island (UHI) [9–11]. Temperature-related studies are critical in the current global warming scenario, where air temperatures in urban areas are also rising due to global warming. [12,13]. One of the reasons for creating UHI is the transformation of natural permeable surfaces into impermeable surfaces [14], which is often the cause of urban outdoor thermal discomfort [15,16]. UHI effects are co-created by the anthropogenic heat

generated by traffic, industry, and domestic buildings (e.g., winter heating, air conditioning in summer), urban geometries (e.g., reduced convection), and other factors [3]. One of the urban design elements that positively modify the urban microclimate [17] is urban green spaces [18–20]. Heat islands contribute to human discomfort, health problems, higher energy bills, and increased pollution. On top of the effects of global warming, heat islands are further reducing the habitability of urban and suburban areas [3,21]. The authors of [22] found statistically significant fine-scale spatial variability in the mortality response to apparent high temperatures. Temperature–mortality relationships were studied in the city of Barcelona [23]. The UHI effect may worsen during heat waves, with projected future increases in extreme climatic events due to global warming [24–26] causing stress on cities and potential threats to human health, which in turn demands effective adaptation measures to alleviate the UHI [27], e.g., by enlarging urban green areas [28].

Several authors emphasize that the urban heat island's effect takes place at night when buildings and streets release the solar heating absorbed during the day [7,29]. Significantly influences of ecological context (defined by biome and elevation) on the amplitude of summer daytime UHI (urban–rural temperature difference) was found by [30], which identified impervious surface area as the primary driver for the increase in temperature, explaining 70% of the total variance in land surface temperature (LST). Results of [31] show more vigorous UHI intensity and enhanced air temperature variability under hot, dry weather types, with the most intense UHIs overnight in dry conditions.

One of the most used indicators of the size of UHIs in urbanized areas is Urban Heat Island Intensity (UHII) [32], which is determined by either comparing the average or the maximum air temperature between an urban and rural area [33]. Assessment of UHI applies both air temperature and surface temperature. Many studies estimated the magnitude of UHI by comparing ground-based observed air temperature in urban and rural weather stations [24,29,31,34], by deploying mobile weather stations [33,35,36], using remote sensing method [37–40] or both [41]. The underpinning data determine whether we evaluate the Surface Heat Island UHISURF or Canopy layer heat island UHIUCL [10], or as used by [38,42] surface UHII (SUHII) or atmospheric UHII. SUHII has the advantage of extracting LST from satellite images and securing data that can cover large areas; this method is not limited by the existence of stations already installed in the place to be studied or to need established by researchers [32]. On the other hand, the limitations include taking pictures at a specific part of the day, image resolution, revisit cycles, clouds, and others [43]. LST from satellite produces a spatially continuous, but time-discontinuous, dataset. The method of obtaining temperatures from stable or mobile monitoring stations (for UHIUCL), in turn, leads to a time-continuous but spatially incoherent data set [44]. According to [45,46], there is no consistent relationship between surface UHII (SUHII) and atmospheric (air) UHII, as [46] states: air temperature UHIs are generally more substantial and exhibit the greatest spatial variations at night, whereas the most significant difference in surface UHIs usually occurs during the daytime. [47] Moreover, surface temperature exhibits much greater spatial and temporal variability than the air temperature. In this study, we focus on remotely sensed land surface temperature (LST) and, consequently, surface UHI.

Various authors have used several approaches, either in the determination of urban and rural areas or in the calculation of SUHII. For extractions of temperatures are used through various platforms such as ASTER, MODIS, NOAA/AVHRR, and LANDSAT [40]. For the distinction between urban and rural parts of the area is often used by the Land Use and Land Cover (LU/LC) layer derived from satellite images, with the proportion of impermeable surfaces often being used as the threshold between them [30,48,49] and/or the administrative boundaries of the city [50].

The UHI effect varies in different areas and depends on city size, land use, topographic factors, vegetation, urbanization and industrialization of the area, the season of the year and time of day, and prevailing meteorological conditions [47]. It is reasonable to expect that the absolute value of the maximum UHI in a city relates to some measure of the size of the city,

like population, city area, or diameter [27,33,51]. Even though, when mentioning the effect of a heat island, we usually imagine large cities [24,41], megacities [34,35], or even urban agglomeration [52], several works confirm the existence of the UHI effect even in medium-sized or small cities [53,54]. The authors of [33] demonstrated the relationship between the size of a village, town or city (as measured by its population), whose populations ranged from 1000 to 2 million inhabitants and the magnitude of the urban heat island they produce.

Understanding the relationships between landscape compositions and landscape configuration, and LST is essential for mitigating the UHI effect. Numerous studies have investigated the impacts of land cover types on LST [46,55–57]. Different representations of LU/LC classes in the urban and its surroundings, and their different configuration can contribute to increasing or decreasing the UHI effect in the city [47,56,58]. The percent cover of buildings the most significantly affects the magnitude of LST, and in contrast, the percent cover of woody vegetation is the most critical factor mitigating UHI effects [46,59]. Many authors confirmed that UHI effects in urban can be mitigated by increasing greenspace cover and optimizing its configuration [60–63]. Vegetation avoids heat build-up by creating shadows and increasing relative humidity through evapotranspiration [64,65]. Urban green infrastructure, defined as the multifunctional network of green spaces that provide multiple environmental, social, and economic benefits to urban areas [66], also has a cooling effect on its surroundings [64,67,68]. These impacts of green space are often referred to as the urban cool island effect [69] or when focusing on park areas as the park cooling islands [54,70]. Green spaces provide many other benefits to humans, such as the reduction of air pollution and noise levels, retentions and water run-off regulation, water purification, carbon storage, acting as a habitat for biodiversity [71–73], and many others [74,75], which have been termed ecosystem services [76–78]. However, different types of green spaces provide a different proportion of ecosystem services [21,75], and, consequently, not all green spaces are likely to offer the same level of mitigation to the urban heat island effect [64,70,79,80]. The authors of [21] found that vegetation types characterized by a more complex structure (trees, shrubs, and herbaceous layers) and by the absence of management (pruning, irrigation, and fertilization) had a higher capacity to provide the ecosystems services of air purification and climate regulation. By contrast, lawns, which have a less complex structure and are highly managed, were associated with a lower capacity to provide these services. The authors of [81,82] confirmed in their research that green areas with tree vegetation have a higher cooling effect than grass areas and areas covered with shrubs. An overview of the results of studies investigating the cooling effect depending on the size and shape of green areas is reported by [67].

In this article, we focused mainly on the summer period with the increasing occurrence of very sweltering days or heat waves, which increase inhabitants' discomfort [83]. We studied the UHI phenomenon in a medium size town of Zvolen (Slovakia) with approximately 41,000 inhabitants, with a minimum area of impermeable surfaces of over 80%, with relatively large woodland in its vicinity, but increasingly summer heat in connection with global climate change. The aims of the article were: (i) to confirm the existence of UHI during summertime in a medium size town surrounded by agricultural and forested landscape, and (ii) to prove the climate mitigation effect on urban green spaces at a statistically significant level as a basis for climate mitigation ecosystem service.

2. Materials and Methods

2.1. Study Area

Zvolen (48°34′4″N latitude, 19°7′24″E longitude) is a medium sized town situated in central Slovakia (Figure 1), 20 km from Banská Bystrica (capital of the region), with an area of 98.73 km^2 and with 40,637 inhabitants. It is located in the Zvolen basin and is surrounded by volcanic mountains from the east, west, and south (the highest peaks in the vicinity are about 600–900 m). The climate type based on the Köpeen–Geiger climate classification for Zvolen features warm-summer humid continental (Dfb) climate. The weather conditions include warm and hot summers and cold, snowy winters. It exhibits four distinct seasons

(winter, spring, summer, and autumn). The coldest month is January, with an average minimum temperature of −8 °C. The warmest months are July and August, with an average maximum temperature of 25.8 °C. The average annual rainfall is approximately 694 mm. In recent years during the summer months, we have witnessed several day periods with high air temperatures in which the maximum daily temperatures exceed 30 °C, which alternate with days with heavy rainfall. According to the Basic Database for the Geographic Information System of Geodesy, Cartography and Cadastre ZBGIS® [84] and Corine Land Cover 2018 [85] layer, the most significant part of the city is covered by discontinuous urban fabric (40%), followed by industrial or commercial units (28%). Continuous urban fabric and roads cover only about 6%, and various forms of more natural surfaces, from grass surfaces, shrubs, parks, and tree lines to forests, cover 33% of the town's area. The remaining areas of the town are under construction, barren land, water areas, etc. Non-irrigated arable land and deciduous and mixed forests predominate in the city's vicinity. The majority of the Slovak urban population (56% of the total 5.5 million population) lives in medium (10–50,000 inhabitants) or small towns (5–10,000 inhabitants). Out of 120 cities and towns in Slovakia, there are only two cities with over 100,000 inhabitants and six cities with approximately 60–90,000 inhabitants. As Slovakia is a mountainous country, the majority of the towns are situated in basins or valleys surrounded by agricultural and forested landscapes. From a national perspective, Zvolen well represents a typical Slovak medium size town.
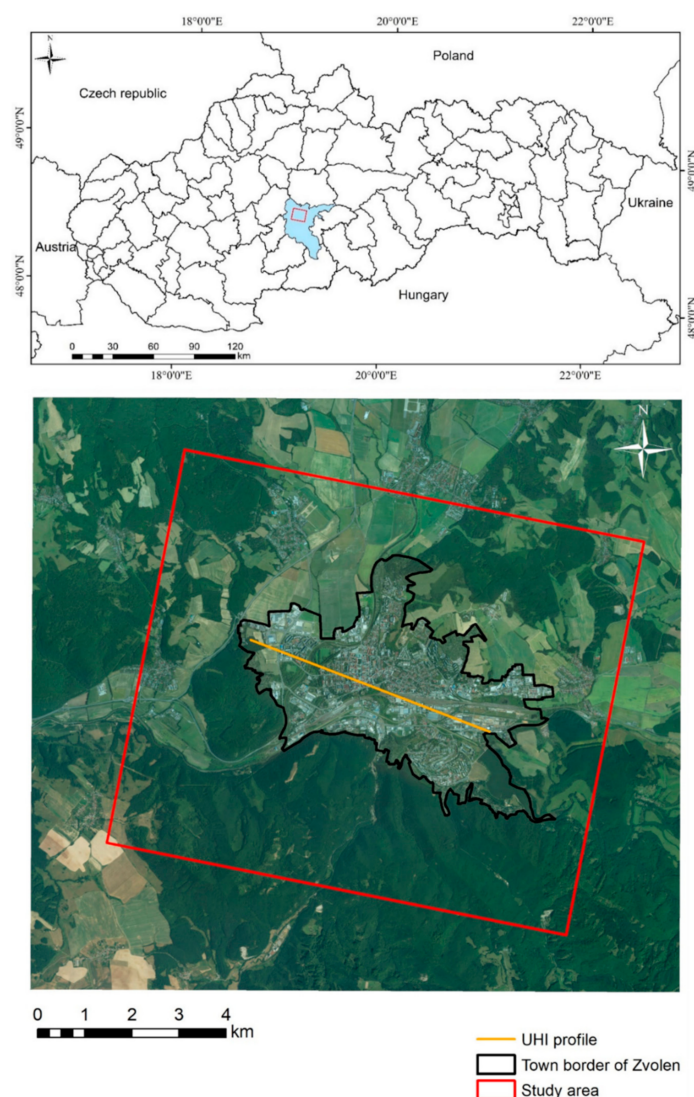

Figure 1. Location of the study area. Note: The town boundary separates the urban zones and the open land.

2.2. Data Sources

For analysis in this study, Landsat images were used to determine land surface temperature and urban heat island for a selected day every year between 2010 and 2021 (11 images). Even though Landsat satellites cross every point on Earth once every 16 days, we cannot research the same day every year. However, Landsat satellites are widely used to monitor and detect environmental changes and are a great source of information from LST and NDVI (Normalized Difference Vegetation Index). Their extensive use has incentivized to develop well-documented techniques for optimal use [86,87]. The data were acquired from the United States Geological Survey (USGS) website [88] and all images have been geographically referenced to the WGS84/UTM projection system 34. Landsat images were selected each year in the summer months of July or August with the minimum cloud cover of the entire Landsat scene (clouds less than 10%). The scan line corrector (SLC) of Landsat 7 failed after 31 May 2003. These products of Landsat 7 ETM+ have data gaps. Therefore, only images without gaps were selected. Specific selected days are listed in Table 1.

The resolution of most Landsat bands is 30 m (panchromatic is 15 m), but it is different for thermal bands. The original resolution of the collected Thermal InfraRed band of Landsat 5 is 120 m, for Landsat 7, it is 60 m, and for Landsat 8, it is 100 m, but in all cases, it has been resampled up to 30 m [89]. Radiometric calibration and correction for atmospheric effects were performed to obtain the surface reflectance and calculate the surface temperature (detailed in Section 2.3). Delineation of the city boundary, urban areas (dense and discontinuous), and urban green spaces (described under Section 2.5) were based on the following spatial datasets: Basic Database for the Geographic Information System of Geodesy, Cartography and Cadastre ZBGIS® [84], orthophotos from 2018 with a spatial resolution (GSD): 25 cm/pixel [90], Corine Land Cover 2018 [85] and four raster datasets of Imperviousness Density from Copernicus European Union's Earth observation program [91] with grid size 20 m for years 2009, 2012, and 2015, and grid size 10 m for 2018. All data were reconciled and rectified to the EPSG: 3035 (ETRS89, LAEA) Coordinate Reference System. Spatial analyses were performed in ArcGIS version 10.3 (ESRI) [92] and statistical analyses in R [93].

Table 1. Acquisition dates and some parameters of the Landsat images used for this study.

Date of Accusations	Satellite	Band Used	Sensor	Resolution	Time (GMT)	Local Time (GMT+1)
14.07.2010	Landsat-5	Band 6	TM/TIRS	30/120	09:23	10:23
09.07.2011	Landsat-7	Band 6	ETM+	30/60	09:26	10:26
27.07.2012	Landsat-7	Band 6	ETM+	30/60	09:27	10:27
14.07.2013	Landsat-7	Band 6	ETM+	30/60	09:28	10:28
02.08.2014	Landsat-7	Band 6	ETM+	30/60	09:30	10:30
13.08.2015	Landsat-8	Band 10	OLI/TIRS	30/100	09:32	10:32
30.07.2016	Landsat-8	Band 10	OLI/TIRS	30/100	09:32	10:32
02.08.2017	Landsat-8	Band 10	OLI/TIRS	30/100	09:32	10:32
04.07.2018	Landsat-8	Band 10	OLI/TIRS	30/100	09:31	10:31
24.08.2019	Landsat-8	Band 10	OLI/TIRS	30/100	09:33	10:33
10.08.2020	Landsat-8	Band 10	OLI/TIRS	30/100	09:32	10:32
28.07.2021	Landsat-8	Band 10	OLI/TIRS	30/100	09:32	10:32

2.3. Land Surface Temperature Retrieval

A single-channel method was used to retrieve the land surface temperature. The thermal band of the Landsat-5 TM and Landsat-7 ETM+ (band 6) was applied to determine the land surface temperature, while Landsat-8 OLI/TIRS was band 10 following [94,95].

The procedure of retrieval can be summarized in four steps:

Calculation of Spectral radiance [94]

$$L_\lambda = \left(\frac{L_{max} - L_{min}}{QCAL_{\max} - QCAL_{min}} \right) \times (QCAL - QCAL_{min}) + L_{min\lambda} \tag{1}$$

where:

L_λ = Spectral radiance at the top of the atmosphere

$QCAL$ = Quantized and calibrated standard product pixel values (DN)

$QCAL_{min}$ = Minimum quantized and calibrated standard product pixel values (DN)

$QCAL_{max}$ = Maximum quantized and calibrated standard product pixel values (DN)

L_{max} = Spectral radiance scaled to $QCAL_{max}$ (W.m^{-2}.sr^{-1}.µm^{-1})

L_{min} = Spectral radiance scaled to $QCAL_{min}$ (W.m^{-2}.sr^{-1}.µm^{-1})

Emissivity: Calculating land surface emissivity (ε) is required to estimate LST since ε is a proportionality factor that scales the black body radiance (Plank's law) to measure emitted radiance, and it is the ability to transmit thermal energy across the surface into the atmosphere. To determine the emissivity, it is necessary to calculate the Normalized Difference Vegetation Index [96]

$$NDVI = \frac{NIR - RED}{NIR + RED} \tag{2}$$

where:

NIR = near infrared band value of a pixel (band 4 for Landsat 5, 7 and band 5 for Landsat 8)

RED = red band value of the same pixel (band 3 for Landsat 5, 7 and band 4 for Landsat 8)

Emissivity (ε):

for $NDVI < 0$ (it is classified as water) then ε = 0.991

$0 < NDVI < 0.2$ (it is classified as bare soil) then ε = 0.966

$0.2 < NDVI < 0.5$ (mixed of soil and vegetation cover—Sparse vegetation) then ε = Equation (3)

$NDVI > 0.5$ (it is classified as vegetation) then ε = 0.973

Following [97]:

$$\varepsilon = m \times P_v + n \tag{3}$$

where: P_v = Proportion of vegetation, m = 0.004 and n = 0.986

$$P_v = \left(\frac{NDVI - NDVI_S}{NDVI_V - NDVI_S} \right)^2 \tag{4}$$

where:

$NDVI$ = Normalized Difference Vegetation Index, derived in Equation

$NDVI_S$ = NDVI value for bar soil (0.2)

$NDVI_V$ = NDVI value for vegetation (0.5).

Atmospheric correction: In the third step, the spectral radiance at the top of the atmosphere (L_λ) was corrected for atmospheric effects using the procedure proposed by [98]:

$$L_C = \frac{L_\lambda - L_\mu - \tau(1 - \varepsilon)L_d}{\tau\varepsilon} \tag{5}$$

where:

L_C = radiance of a blackbody target of kinetic temperature

L_λ = spectral radiance at the top of the atmosphere

L_μ = upwelling radiance

τ = atmospheric transmission

ε = emissivity

L_d = downwelling radiance

The values of L_μ, L_d, and τ for an image from a specific date and location were calculated using an Internet application available at (http://atmcorr.gsfc.nasa.gov/, accessed on 6 April 2022).

Calculation of land surface temperature in Celsius [94]

$$T = \frac{K_2}{\ln\left(\frac{K_1}{L_T} + 1\right)} - 273.15 \tag{6}$$

where:

T = land surface temperature in °C.
K_1 = Band-specific calibration constant in W/m^2 sr µm from the metadata (Table 2)
K_2 = Band-specific calibration constant in Kelvin from the metadata (Table 2)
L_C = Spectral radiance (W/m^2 sr µm)

Table 2. Thermal band calibration constants for specific Landsat satellites.

	Band	K_1	K_2
Landsat-8 OLI/TIRS	Band 10	774.8853	1321.0789
Landsat-7 ETM+	Band 6	666.09	1282.71
Landsat-5 TM	Band 6	607.76	1260.56

2.4. Urban Heat Island and Urban Heat Island Intensity Retrieval

The authors of [33] defined Urban Heat Island Intensity (UHII) by comparing the average air temperature between an urban and a rural area. In this paper, we assess Surface Urban Heat Island Intensity (SUHII):

$$SUHII = T_{urban} - T_{rural} \tag{7}$$

where:

$SUHII$ = Surface Urban Heat Island Intensity
T_{urban} = Average land surface temperature (LST) of the urban area
T_{rural} = Average land surface temperature (LST) of rural area

We were interested in the differences between the most built-up parts of the town and its unbuilt surroundings and the differences within the town between zones with different proportions of impervious surfaces (detailed in Section 2.5). Therefore, we evaluated the statistical significance of the differences in the average temperature between the individual zones of the town and the undeveloped open landscape around the town using a one-way ANOVA (detailed in Section 2.6).

For spatial assessment of SUHII, we applied the formula by [44]:

$$sSUHII = \frac{T_i - T_a}{T_a} \tag{8}$$

where:

$sSUHII$ = space Surface Urban Heat Island Intensity
T_i = land surface temperature (LST) at one site
T_a = average land surface temperature of the whole area.
The results were classified into five SUHII classes (Table 3).

Table 3. Classification of the surface urban heat island intensity (following [44]).

SUHI Intensity Levels	
<0	No SUHII (Green Island)
0–0.1	Weak heat island
0.1–0.2	Medium heat island
0.2–0.4	Strong heat island
>0.4	Extremely strong heat island

2.5. Spatial Delineation of Urban Zones

The delineation of a town and its zones consisted of several consecutive steps. First, we allocated the administrative boundaries of the town based on the Cadastre of Real Estate from the Basic Database for the Geographic Information System of Geodesy, Cartography, and Cadastre ZBGIS® [84], thereby separating the town area and the surrounding open (rural) land (Figure 1). We then divided the town area into three zones based on the percentage of impervious surfaces by the Copernicus imperviousness density data: (a) dense urban area (UA) with 31–100% impervious surfaces, (b) discontinuous urban area (SU) with 1–30% impervious surfaces, and (c) urban green spaces (UGS) with 0% impervious surfaces. We considered only undeveloped areas (impervious surfaces and water bodies were excluded) beyond the town limits (up to a distance of 3 km) as the open land (OL) surrounding the town. Since the spatial extension and arrangement of areas with different degrees of imperviousness changed during the evaluated period, we updated the individual urban zones and the surrounding open land and for the analyzed periods based on the Copernicus imperviousness density data from the years 2009, 2012, 2015, and 2018 (Figure 2). We evaluated the differences in surface temperature between zones in a specific year for zones based on the Copernicus imperviousness density data from the year closest to the estimated period (Figure 3).
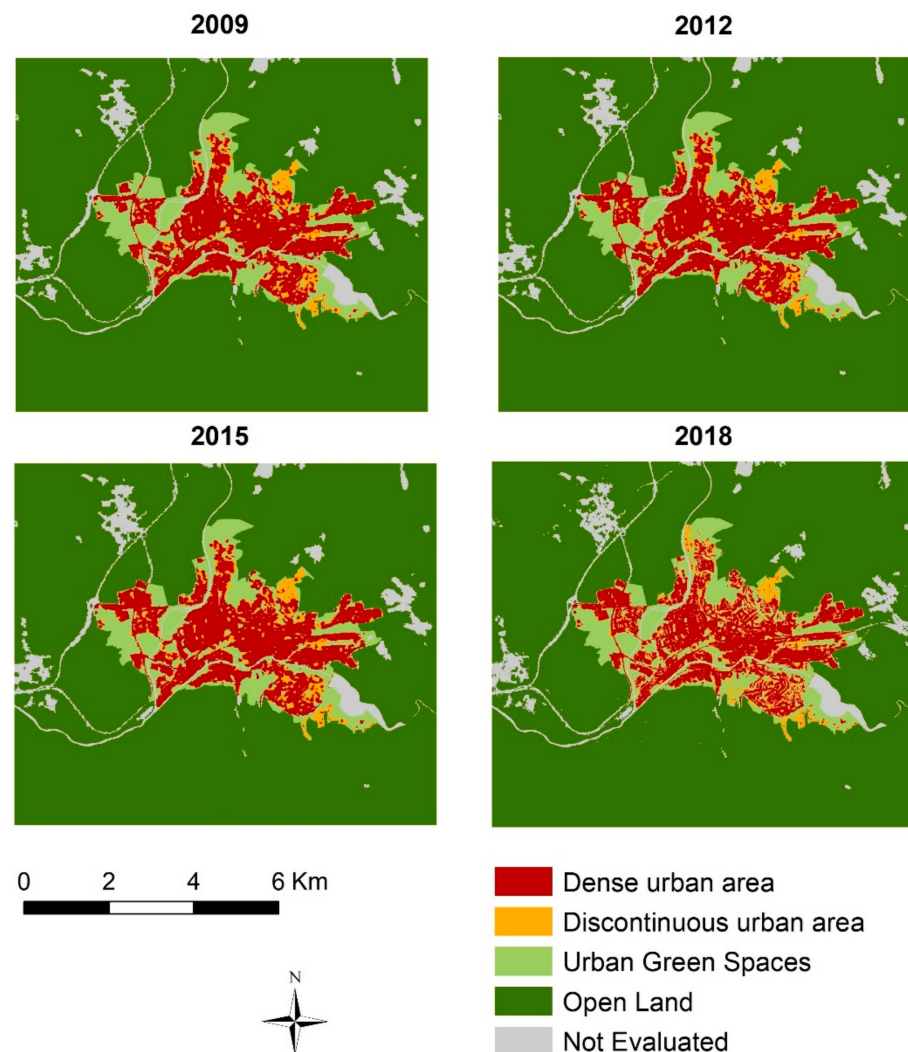

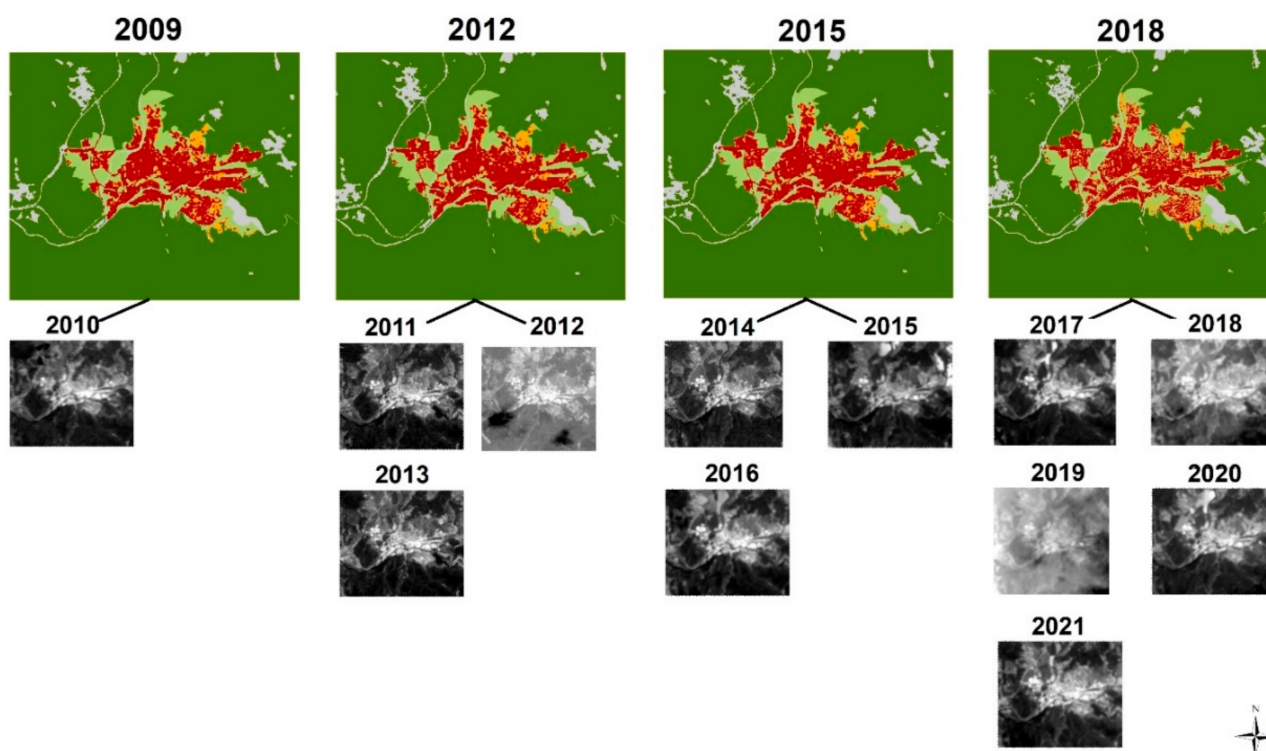**Figure 2.** Urban zones in the respective years.

Figure 3. Assignment of LST calculated from Landsat images of a specific year to urban zones defined based on the Copernicus imperviousness density data according to the year closest to the evaluated period.

2.6. Statistical Analysis

First, we generated 300 random points (1200 points in total) for each of the 4 allocated zones (3 urban zones and one open land) using the ArcGIS tool "Create Random Points". Water bodies and cloud-covered areas were excluded from generating random points in each zone. Since we had four updated zone layers (Figure 2), four different groups of random points were also developed for the years 2009, 2012, 2015, and 2018. Using the ArcGIS tool "Extract Multi Values to Points", calculated LST values from LANDSAT images. In contrast, temperature values from a specific year were extracted into a group of points according to the scheme shown in Figure 3. Differences in LST between the urban zones and the open land were tested with a one-way analysis of variance (ANOVA) followed by post hoc comparisons using the Tukey HSD method after checking the homogeneity of variances using the Bartlett test [99]. In general, ANOVA includes a whole group of methods, but in its simplest form, it tests the null hypothesis of equality of means between several independent groups by comparing the variability between them. ANOVA tests the null hypothesis that there are no differences between the means of the values of several groups. If the variability between groups is improbably large (we test with an F-test), then we reject the null hypothesis of equality of means and consider groups to be different [100–102].

3. Results and Discussion

3.1. Analysis of Land Surface Temperature

The study analyzed a total of 11 years of data concentrated on the summer months of July and August, one selected day each year, because, in the summer, the heat island effect can be combined with the increasingly frequent occurrence of heat waves, which leads to temperature stress in people, and threats to health and quality of life. The comparison of LST within the study area for individual years, the range of values, maximum, minimum, and average temperature can be seen in Figure 4. Temperatures are calculated for the time around 11:30 Central European Time (Table 1), the time of the Landsat satellite overflight. The average temperature on summer days was usually around 20–25 °C, minimum surface temperatures (water bodies, forest) were usually around 14–16 °C, and maximum temperatures

(impermeable surfaces–buildings, parking lots) reached about 40 °C, in in 2018, the maximum LST even exceeded 40 °C. Only two cooler days occurred in 2012 (minimum LST below 10 °C and maximum just above 30 °C) and especially the evaluated day in 2019 with minimum LST below 5 °C (water reservoir) and maximum temperature up to 25 °C.
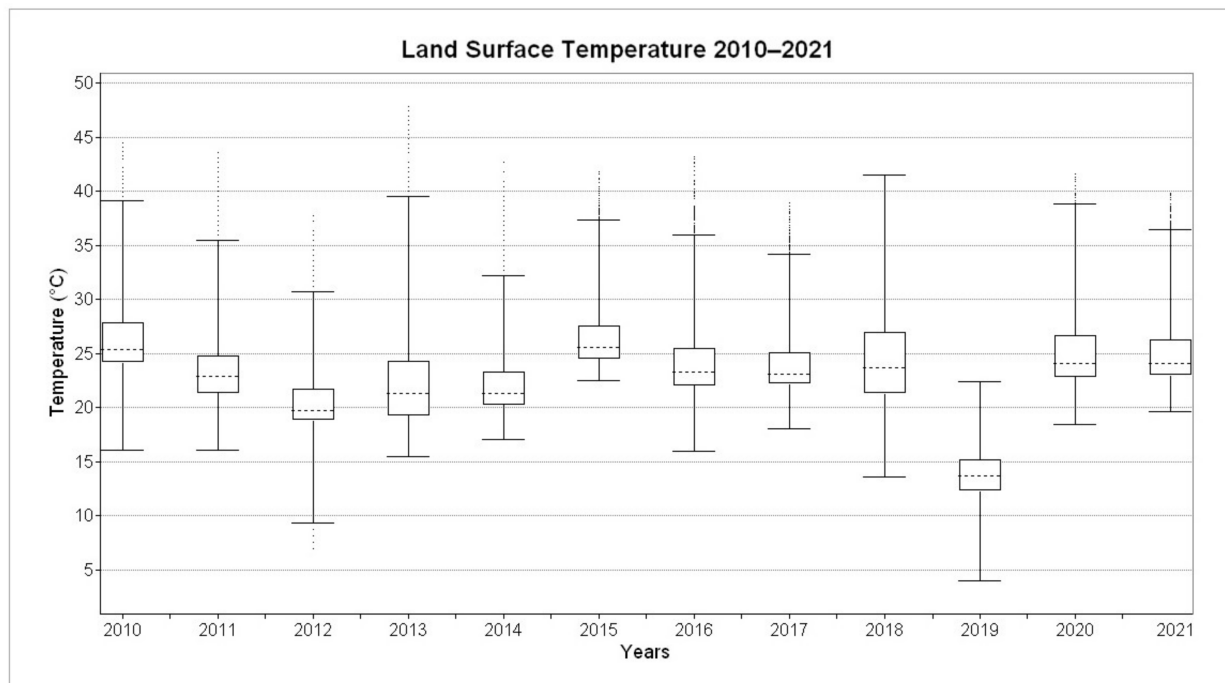

Figure 4. Distribution comparison of LST calculated from Landsat images for evaluated days (Table 1) in 2010–2021. Boxes indicate median and quartiles, and whiskers extend to the most extreme data points, not considering outliers (defined by 1.5 interquartile ranges).

The spatial distribution of LST on the evaluated days for individual years in the study area is shown in Figure 5 (2010–2015) and Figure 6 (2016–2021). The images show that the highest LST values are always within the town boundary, except for the significantly coldest day (in 2019) when the difference between the town and the open land is not so obvious. It can also be seen from the calculated values that the LST difference between the town and the surrounding open land is more pronounced on warmer days. That is, the warmer the day was, the more pronounced the temperature difference can be observed between those two areas. Conversely, on colder days, this difference is smaller. The spatial pattern of temperature distribution is similar. At first glance, several characteristic areas with particularly elevated LST values stand out. These are all industrial areas and the most built-up parts of the town. Changes in land use are also reflected in the details around the town. Mainly the cultivation of different crops in the fields in other years, when the areas covered by a small percentage of vegetation have a similar LST value to the impervious areas in the town (e.g., the North-Eastern part of the territory in 2015). Similar results were found in several studies [56,59,103], where barren land has identical or higher LST values than the warmest settlement areas. On the other hand, the southeastern edge of the town, surrounded by forests, was significantly cooler for the entire period.
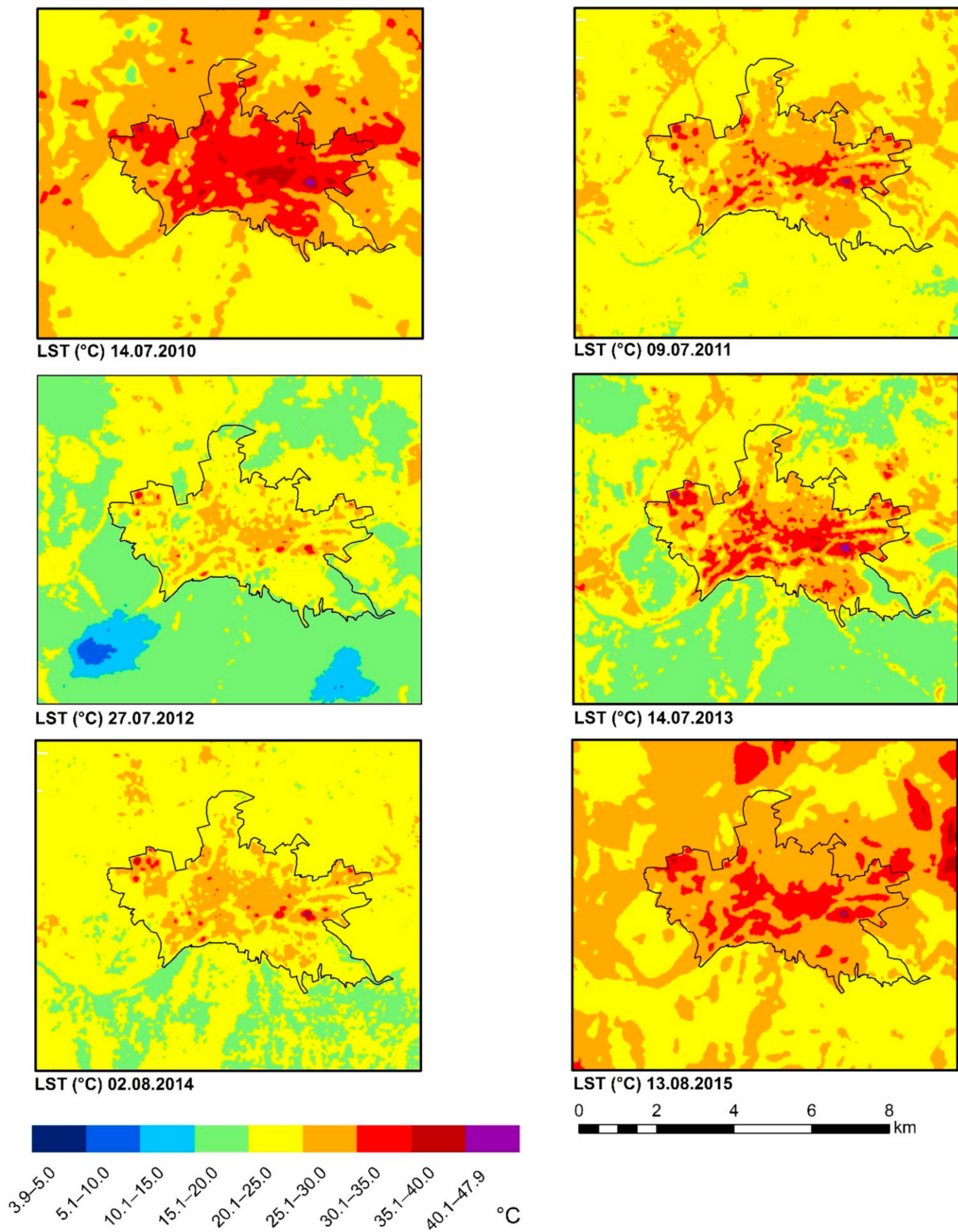
Figure 5. Calculated LST values for evaluated days between the years 2010–2015. Note: Blue blobs (temperatures under 15 °C) in 2012 were covered by clouds.
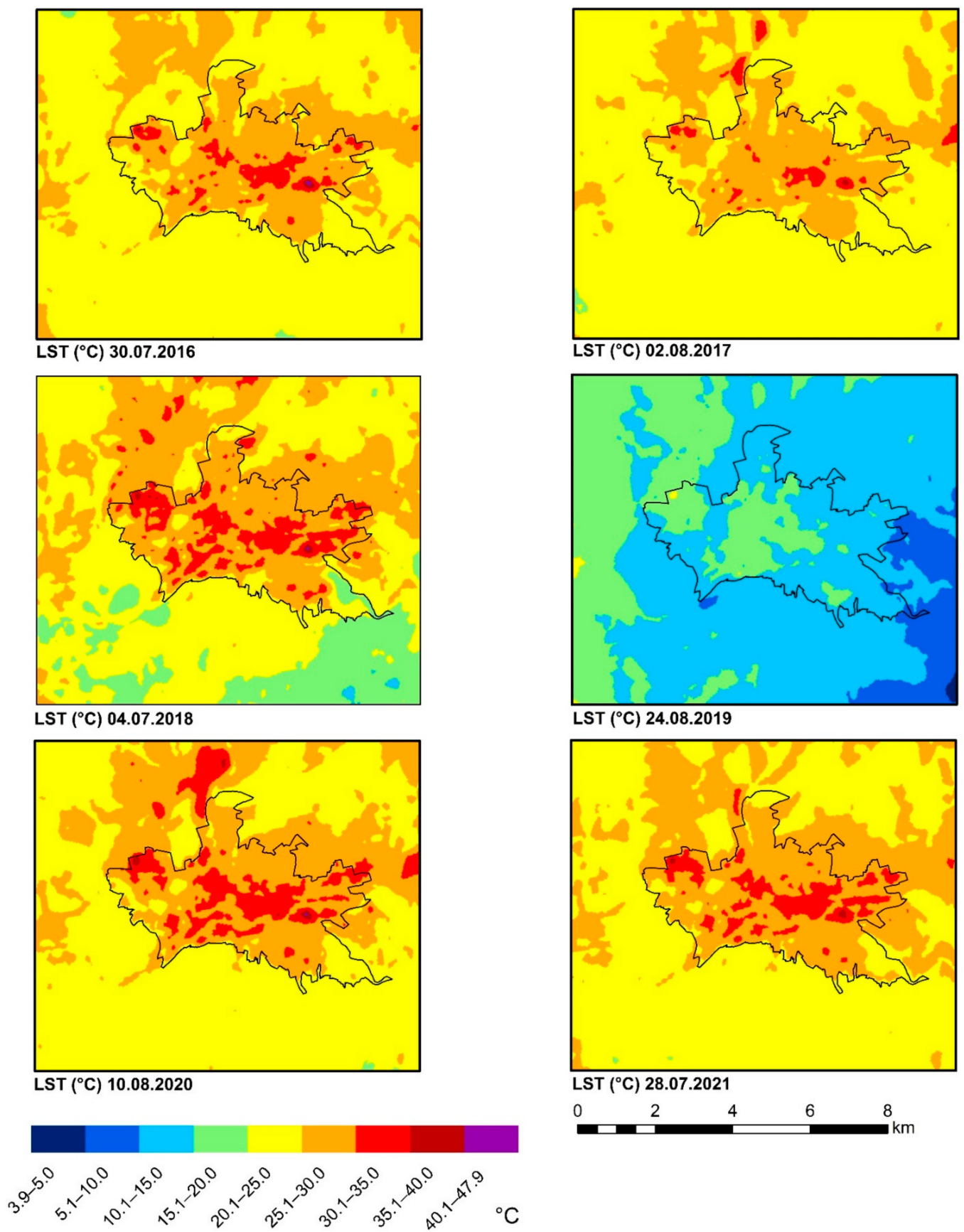
Figure 6. Calculated LST values for evaluated days between the years 2016–2021.

3.2. Evaluation of the Spatial Pattern of Surface Urban Heat Island

To display LST changes within the town on a transect from areas with a 0% share of impervious areas (green areas) to industrial and built-up areas with a share of impervious areas over 80%, we translated a profile (Figure 1) passing through the town territory from northwest to southeast. It starts in the forest and passes through residential areas, wetlands (watered meadows), urban green areas, and industrial areas. Figure 7 shows the course of LST on the profile line for individual years. The temperatures are the highest in the places passing through the industrial zone and the most built-up parts of the town; on the contrary, the temperatures are several degrees lower in the places where the profile passes through the urban green spaces. The differences are significant, except for the temperatures detected during the day in 2019, which was significantly cooler than the other evaluated days.
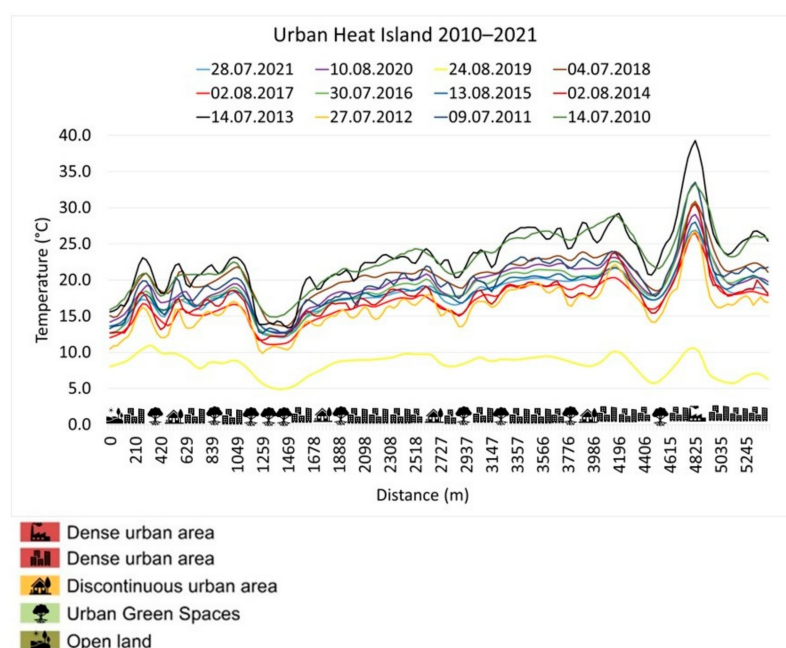

Figure 7. The course of LST on the profile line for individual years in 2010–2021.

In accordance with the above calculation (10), SUHII is usually determined as the difference in average temperatures for urban and rural parts of the area obtained from satellite images. Still, other approaches are also used to highlight the magnitude of the difference. For example, in [104], this temperature difference is further divided by the temperature of the rural parts of SUHII; in [105], urban heat island was identified as places with a temperature higher than 0.5 times the standard deviation (σ) above the average (μ) temperature of the territory SUHII = LST $> \mu + 0.5\sigma$ and [106] define the size of SUHII using the magnitude of the slope of the linear regression dependence between land surface temperature and the percentage of artificial impervious cover.

To express the spatial pattern of SUHII (spatial pattern of SUHII (eSUHII)), we used the method described by Xu et al. They expressed SUHII as the ratio of LST at one site (T_i) minus the average LST of the assessed area (T_a) divided by the average LST of the assessed area (see Equation (8) and Table 3).

Spatial expression of UHI intensity (sSUHII) is presented in Supplement SA1 (2010–2015) and Supplement SA2 (2016–2021). sSUHII expresses how much the LST of a specific area differs from the average LST in the area. Areas with lower or equal average LST are evaluated as areas without SUHI ([44] calls them Green Island). The more the LST of the area differs from the average value in the area, the higher the intensity of SUHI (Table 3). As can be seen from the calculated values of the area without SUHII, they are linked to areas outside the town limits covered with forests or other dense vegetation. On the contrary, the highest intensity of SUHI in the town is achieved in the areas with the highest proportion of impervious

surfaces (industrial zone and the most built-up parts). From the comparison of individual days within different years, it is also possible to observe that the intensity of SUHI and its spatial distribution strongly depend on the temperatures reached.

3.3. Comparison of SUHII Differences between Urban Zones with Each Other and between Urban Zones and Open Land

From the previous calculations and looking at Figures 5, 6 and 8–10, we can see that areas with a high degree of coverage by impervious surfaces have higher LST values than urban green spaces on summer days. However, is this difference statistically significant? We verified this hypothesis using the one-way ANOVA method (detailed in Section 2.6) by comparing LST for 300 random points for each of the three zones of the town—UA, SU, UGS and LST of 300 random points from around the town—OL.
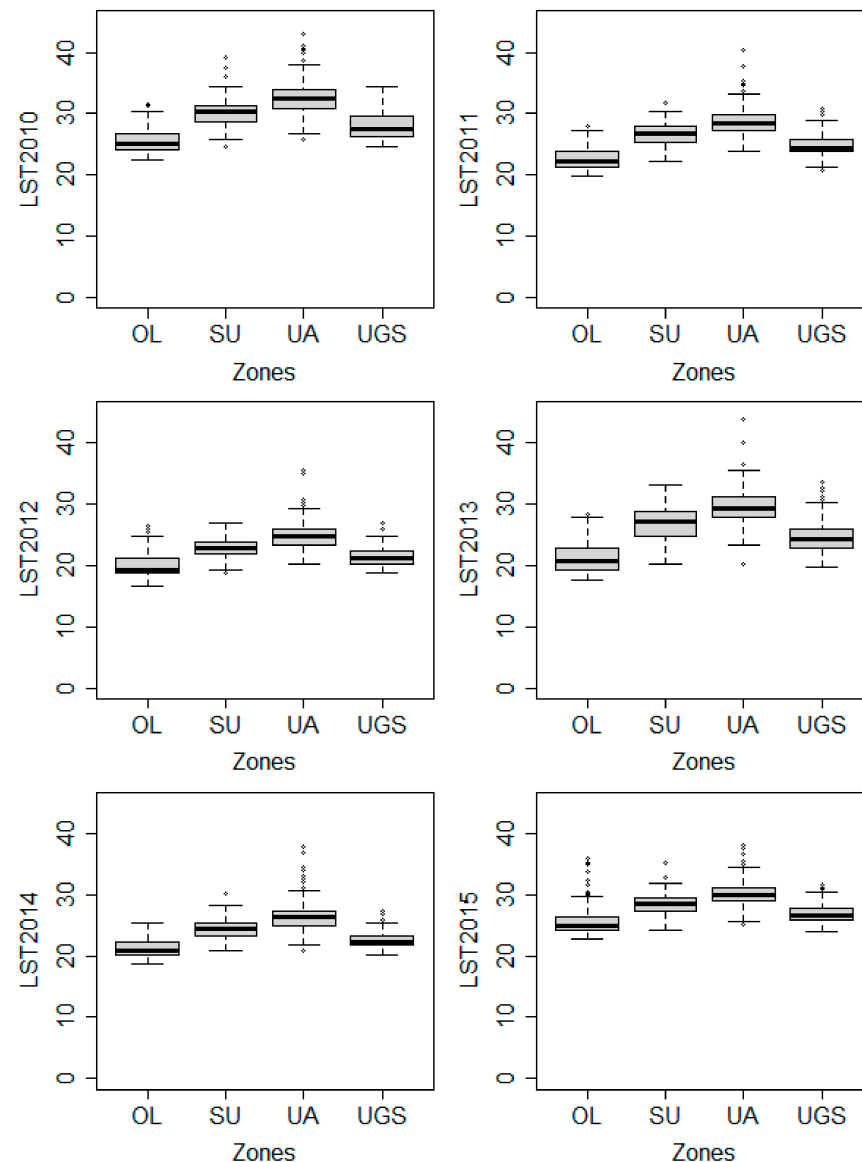

Figure 8. Comparison of boxplots of LST distributions for random points within the analyzed zones in the years 2010–2015. Boxes indicate median and quartiles, and whiskers extend to the most extreme data points, not considering outliers (defined by 1.5 interquartile ranges). OL—open land, UA—dense urban area, SU—discontinuous urban area, UGS—urban green spaces.

Figure 9. Comparison of boxplots of LST distributions for random points within the analyzed zones in the years 2016–2021. Boxes indicate median and quartiles, and whiskers extend to the most extreme data points, not considering outliers (defined by 1.5 interquartile ranges). OL—open land, UA—dense urban area, SU—discontinuous urban area, UGS—urban green spaces.
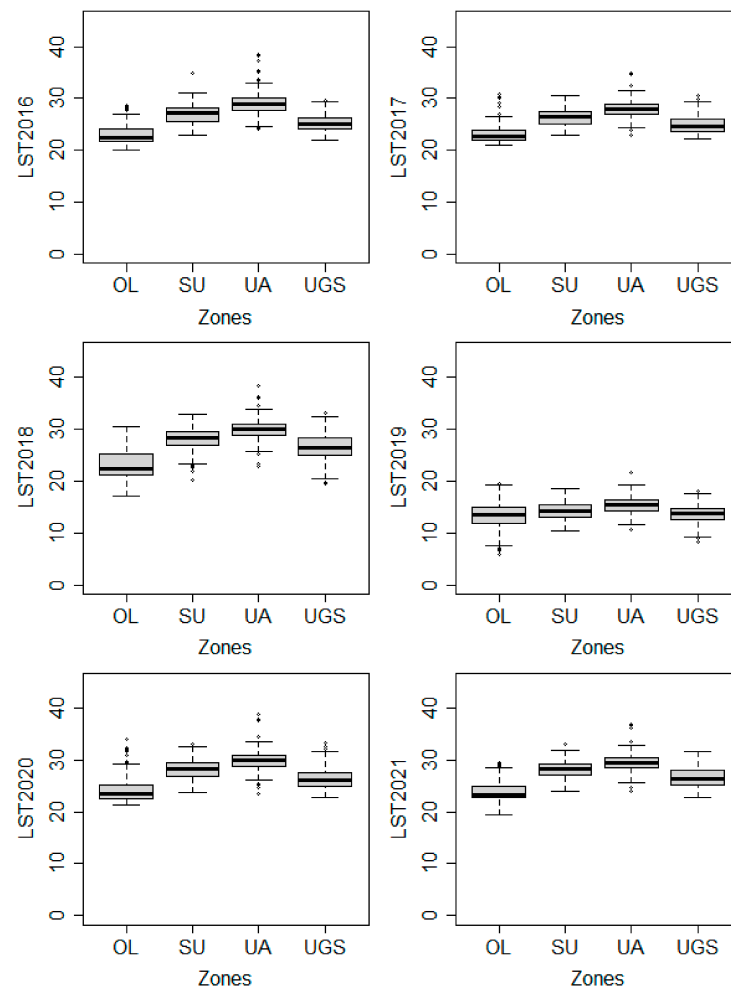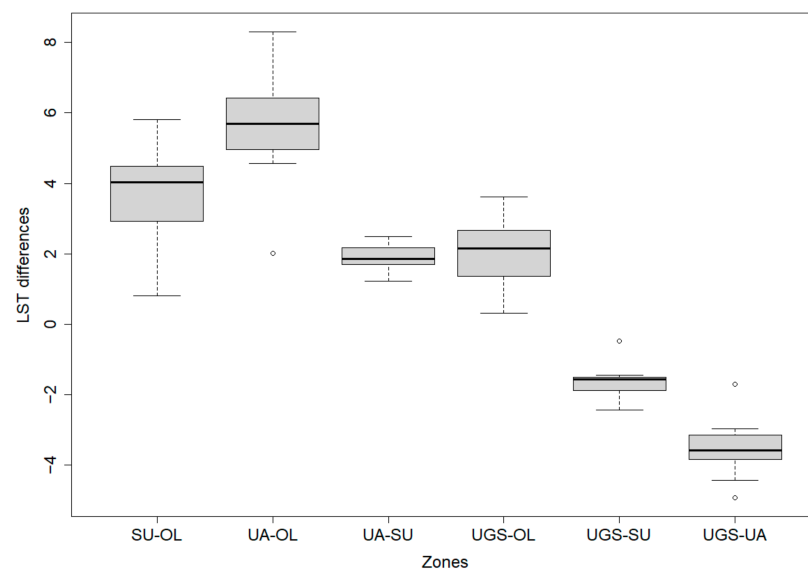

Figure 10. Comparison of average LST differences between pairs of zones for the entire evaluated period.

A comparison of the average, minimum, and maximum LST between the four zones for individual evaluated days during the years 2010–2021 is shown in Figure 8 (2010–2015) and Figure 9 (2016–2021). Based on one-way ANOVA followed by post hoc comparisons using the Tukey HSD method, we can conclude that the differences in LST between the four compared zones differ statistically significantly in all years and between all groups with each other, with one exception in 2019, in the day, which was mainly the coldest of all evaluated days (Table 4). The results confirmed that the average LST in UA is the highest of all zones on all days of the entire evaluated period and that it significantly ($p < 0.001$) differs from the LST of the other zones. This result confirms the existence of UHI during summertime in medium town Zvolen. The second warmest zone on all days of the evaluated period was SU, which differs significantly ($p < 0.001$, or in one case $p < 0.01$) from the LST in the other zones. The third in order in terms of LST height is UGS, who's average LST is significantly ($p < 0.001$, or in one case $p < 0.01$) lower than the average LST in UA and in SU. This result gave us a positive answer to our second research question that urban green areas at a statistically significant level mitigate UHI in the town and have the capacity to provide the climate mitigation ecosystem service.

On the other hand, LST in UGS is significantly ($p < 0.001$) higher than the average LST in OL on all days during the entire observed period (with one exception in 2019). On this significantly coldest day of all evaluated days, no statistically significant difference was observed in the average LST of UGS and the average LST of OL. The OL zone during the entire monitored period had an average LST significantly lower than all town zones (except for one case mentioned above), which confirms the hypothesis of the existence of the UHI effect during the summer months, even in a medium size town as Zvolen.

However, the significance of LST differences between individual zones must also be evaluated in the context of the accuracy of LST determination from Landsat images by individual methods, which we do in the next part.

Table 4. A significance level of the F-test in one-way ANOVA and multiple comparisons of differences between pairs of zones in the territory using the Tukey HSD test.

Date	F (3, 1196)	p (ANOVA)	Difference between Zones (p-Value of Post-Hoc)					
			SU–OL	UA–OL	UGS–OL	UA–SU	UGS–SU	UGS–UA
14 July 2010	616.1	<0.001	<0.001	<0.001	<0.001	<0.001	<0.001	<0.001
9 July 2011	577.6	<0.001	<0.001	<0.001	<0.001	<0.001	<0.001	<0.001
27 July 2012	440.1	<0.001	<0.001	<0.001	<0.001	<0.001	<0.001	<0.001
14 July 2013	595.8	<0.001	<0.001	<0.001	<0.001	<0.001	<0.001	<0.001
2 August 2014	537.2	<0.001	<0.001	<0.001	<0.001	<0.001	<0.001	<0.001
13 August 2015	409.2	<0.001	<0.001	<0.001	<0.001	<0.001	<0.001	<0.001
30 July 2016	654.9	<0.001	<0.001	<0.001	<0.001	<0.001	<0.001	<0.001
2 August 2017	505.2	<0.001	<0.001	<0.001	<0.001	<0.001	<0.001	<0.001
4 July 2018	476.9	<0.001	<0.001	<0.001	<0.001	<0.001	<0.001	<0.001
24 August 2019	72.8	<0.001	<0.001	<0.001	0.145	<0.001	0.006	<0.001
10 August 2020	474.4	<0.001	<0.001	<0.001	<0.001	<0.001	<0.001	<0.001
28 July 2021	555.6	<0.001	<0.001	<0.001	<0.001	<0.001	<0.001	<0.001

F (3, 1196)—values of F statistic, *p*—significance level, OL—open land, UA—dense urban area, SU—discontinuous urban area, UGS—urban green spaces.

3.4. Evaluation of the Magnitude of SUHII differences between Zones

The average differences between the LST of individual zones for the entire monitored period and their 95% family-wise confidence level are shown in Supplement SB1 (2010–2017) and in Supplement SB2 (2018–2021). The average values of the differences for the entire evaluated period are shown in Figure 10. The difference in average LST between UA and OL ranges from 2.0 ± 0.38 °C in 2019, the coldest of all days of the evaluated period, to 8.3 ± 0.53 °C in 2013, with an average with a difference value of 5.6 °C. These results are in accordance with the findings of [30], who emphasizes the importance of the "ecological context" (biome), significantly influencing the amplitude of the summer daily UHI (urban-rural temperature difference), which is the largest (mean 8 °C) observed for cities built in biomes dominated by

temperate deciduous and mixed forest. The authors of [33] found the air temperature difference between the city of Montreal (2 million inhabitants) and its surroundings from 6.7 °C to 9.7 °C. In the town of St. Hyacinthe (23,600 inhabitants in 1971), the air temperature difference was from 3.8 °C to 6 °C.

UGS was cooler (their average LST was lower) during the evaluated period compared to UA from -1.71 ± 0.38 °C in 2019 to -4.94 ± 0.53 in 2013, with an average with a difference of -3.5 °C for the estimated period. According to the findings of [107], average LST in Jinan, China, urban parks was approximately 3.6 °C lower than that of the metropolitan area, with the most significant temperature difference of 7.84 °C occurring during summer daytime. As demonstrated in an example from Beijing by [108], the average difference between green spaces and the average thermal condition of impervious surface on an August day was approximately 2 °C. The authors of [109], in the city of Port Phillip, Australia, during the day in warm summer conditions, found that with an increase in vegetation cover by 10%, there was a decrease in LST by 1.2 °C. The authors of [87] established that for a 10% increase in the amount of green area, there was a 1.3 °C reduction in LST in Rotterdam, Netherlands. In contrast, the authors of [110], in Worcester County, Massachusetts, assessed the effects of reduced tree cover on LST and found that a 10% loss in tree canopy cover caused a 0.7 °C increase in LST and a 10% increase in a sub-canopy impervious surface area exposed due to tree loss caused 1.66 °C increase in LST. [111] found that the parks, depending on their size, were colder than the surrounding area from 2.3 to 4.8 °C, and their cooling manifested at a distance of 85–284 m. Similarly, the authors of [54], in Wroclaw (Poland), found a difference between the temperature of the park and its surroundings from 1.9 to 3.6 °C depending on the park size, forest area, and land use type in the park's vicinity, with the cooling distance varied from 110 m to 925 m. For example, the authors of [112] found that wetlands affected built-up area, farmland, and road up to 381, 321, and 347 m, respectively. A negative impact on local environmental conditions due to new urbanization is reported by [113,114].

The difference in average LST between SU and OL was from 0.8 ± 0.38 °C on the coldest of the evaluated days in 2019 to 5.8 ± 0.53 °C in 2013, the average value of the difference for the evaluated period was 3.8 °C. The average values of LST UGS compared to LST OL were always statistically significantly higher, except for the year 2019, when there was almost no difference between them at 0.31 ± 0.38 °C. Conversely, the highest difference was recorded in 2013, when it was up to 3.37 ± 0.53 °C. On average, the LST of UGS was 2 °C higher than the average LST of OL. The average LST difference between UA and SU is similar to the comparison between UGS and OL. On average for the evaluated period, the average LST of UA was almost 2 °C higher than the average LST of SU. The minimum difference between them of 1.22 ± 0.38 °C was on the coldest day of the entire evaluated period in 2019, and the highest distinction of 2.49 ± 0.53 °C was found in 2013. The average LST value of UGS was always significantly lower than the average LST of SU for the entire evaluated period. As in previous cases, the most inferior difference -0.48 ± 0.38 °C was found on the coldest of all evaluated days, in 2019. The highest difference -2.45 ± 0.53 °C was discovered in 2013. The average difference for the evaluated period was -1.7 °C.

The authors of [115] analyzed the development of surface urban heat islands (SUHI) and compared LST changes within 617 functional urban areas in Europe in 20 years. They found that urban and industrial land uses have significantly higher LST than green urban areas across all years (about 4 to 6 °C), as do agricultural areas within cities, emphasizing the influence of geographic location (latitude) on the size of the differences. Similarly, the authors of [116] analyzed in detail the contribution of different functional construction land zones to the UHI effect by comparing the average LST of the construction land zone and the LST of the forest (outside the city) in Shenzhen, China. They found that the areas with manufacturing function exceed the average LST of the forest the most, by 3.99 °C on average. They are followed by warehousing and logistics function with 3.69 °C and areas with street and transportation function with 3.61 °C higher average LST than forest. Areas

with administration and public services functions were warmer than the forest by 2.54 °C and areas with residential parts by 2.21 °C.

From the boxplots in Figure 10, we can also see that the variability of the average LST difference between pairs of zones within the evaluated days is more significant in the pairs where open land figures. It can be assumed that it caused by a greater variety of surfaces present in OL compared to cases where UA and SU or UGS and SU are compared.

Several authors have addressed the accuracy of LST determination from Landsat images using different calculation algorithms by comparing with reference surface measurements at the same points [117–119]. All cited works state that even though all algorithms achieve good results, the Single-Channel Algorithm (which we used in our calculation) usually achieves somewhat lower accuracy compared to e.g., Mono-Window Algorithm or Split-Window Algorithm. In general, the authors of [120] mention three sources of error when determining LST from satellite images. The first comes from sensor properties (calibration, assumption from broad band to single band) with error approx. 0.6 K, the second from atmospheric correction (error approx. 0.5 K), and the third from estimating surface emissivity (error approx. 0.2 K). The authors of [117] report the accuracy of Single-Channel Algorithm based on Root Mean Square Error (RMSE) for four selected energy balance monitoring sites from the Surface Radiation Budget Network (SURFRAD) from 1.61 K (Cropland), through 1.47 K (Grassland), 1.33 K (Leaf Forest), to 1.26 K (Rural Land). [121] stated for Single-Channel Algorithm RMSE value 1.7 K. The authors of [122] report RMSE values from 2.61 K (atmospheric transmission was less than 0.3) to 0.51 K (atmospheric transmission is at least 0.85), depending on different atmospheric conditions. Since the days evaluated by us were almost cloudless, we can assume, even in the context of other works, that the degree of accuracy of our calculations (which will need to be verified by measurements in the future) is around 1.7 °C. Then we can evaluate LST differences between zones up to 1.7 °C with caution (even with a 95% family-wise confidence level of LST differences between pairs of zones) and differences between pairs of zones: UA–SU, UGS–OL, UGS–SU (Figure 10) can only be considered evident on days with the highest daily temperatures, when the differences significantly exceeded 1.7 °C. In Supplement SC, we list the years in which the difference between zones may not be evident, taking into account the possible errors of LST determination. On the other hand, the differences between the pairs: UA–OL, SU–OL, and UGS–UA are evident even after taking into account this degree of accuracy in all evaluated days except for 2019, which was a significantly cooler day compared to all other evaluated ones. On this day, the highest calculated LST was only 22 °C, while on the other evaluated days it reached up to 35 °C (Figures 5 and 6).

4. Conclusions

Based on the results, we can answer positively to both of our study questions, even when taking into account the accuracy of the LST calculation. The study confirmed the existence of the UHI effect during the summer months between 2010 and 2021, even in such a medium size town as Zvolen—a town with a minimum area of impermeable surfaces of over 80%, without skyscrapers, and with relatively large woodland in its vicinity. The average LST of the town was statistically significantly higher than the LST of the surrounding open land. The temperature difference depended on the town surface coverage, and compared to LST of the open land, we can arrange the evaluated parts of the town in descending order as follows: (i) UA was on average warmer by 5.6 °C (compared to LST of the OL), (ii) SU was on average 3.8 °C warmer (compared to LST of the OL), and (iii) UGS were on average 2 °C warmer (compared to LST of the OL).

The capacity of urban green spaces to mitigate the local climate and provide climatic ecosystem service was also confirmed. The LST of the UGS on all days of the evaluated period was significantly lower than the LST of other town zones. The most significant difference was, in accordance with the assumptions, compared to UA, where UGS was cooler on average by 3.5 °C during the evaluated period. Compared to SU, UGS was cooler on average by 1.7 °C. UA had a significantly higher average LST by almost 2 °C,

even compared to SU, within which there is a more excellent representation of vegetation (gardens, lawns, tree alleys, etc.). When taking into account the accuracy of the LST calculation using the Mono–Window Algorithm, we must evaluate the significance of LST differences between zones up to 1.7 °C (with the inclusion of a 95% family-wise confidence level of LST differences between pairs of zones up to 2.3 °C) with caution. Based on the above, it can be concluded that there is a statistically significant difference between OL and UA, as well as between OL and SU. It is also possible to state a statistically significant cooling effect of UGS compared to UA, as well as compared to SU. The difference between the other zones cannot be confirmed after taking into account the LST calculation error. From the results it can be seen that the differences between individual zones increase with the reached temperature during the day and become significant (Supplement SC).

This study brings only the preliminary results about the temperatures of zones in Zvolen. It will be necessary to carry out verification measurements in situ and take into account other parameters. For example, the authors of [123] evaluate the influence of building shadows on LST, whose area and distribution display strong seasonal variations that significantly influence the urban land surface temperature (LST). They also emphasize taking into account the heterogeneity of individual pixels of satellite images (e.g., for Landsat 8 100 m pixel resampled to 30 m) for which LST is calculated. It will also be necessary to classify urban green spaces into types in more detail and to determine the effectiveness of individual types and their percentage representation for UHI mitigation.

We analyzed the UHI under clear sky conditions, mainly because UHI manifestations are more pronounced during cloudless days. On the other hand, it is also true that the existence of clouds makes it difficult to obtain the surface thermal environment during cloudy days. However, the frequent appearance of clouds in our (and especially more northerly) latitudes makes it necessary to overcome this obstacle. Some recent studies [124,125] aiming at reconstructing the LSTs of cloudy pixels are good options for further analysis.

We note that our results only assess the incidence of SUHII during the day. At the same time, temperature conditions during the night are also essential for people's health. For many people, and not only seniors, very warm and sultry summer nights, which do not provide thermal relief, can be challenging. Therefore, in the following research, we plan to focus on evaluating the intensity of the UHI effect during the night using mainly mobile air temperature measurements.

The quantification of the climate mitigation capacity of vegetation to provide climate mitigation ecosystem service can be directly applied in the management of existing urban green spaces or in planning new green infrastructure elements. It is of critical importance since summer heat waves are more frequent due to climate change, and as shown in this study, the UHI manifests even in medium size towns.

Conflicts of Interest: The authors declare no conflict of interest. The funders had no role in the design of the study; in the collection, analyses, or interpretation of data; in the writing of the manuscript; or in the decision to publish the results.

References

1. Continuing Urbanisation. Available online: https://knowledge4policy.ec.europa.eu/continuing-urbanisation_en (accessed on 10 June 2022).
2. Marzluff, J.; Shulenberger, E.; Endlicher, W.; Bradley, G.; Simon, U.; Alberti, M.; Ryan, C.; ZumBrunnen, C. *Urban Ecology–An International Perspective on the Interaction between Humans and Nature*; Springer: New York, NY, USA, 2008; 807p.
3. Gartland, L. *Heat Islands. Understanding and Mitigating Heat in Urban Areas*; Earthscan; Routledge: London, UK, 2008; 215p.
4. Dadvand, P.; Bartoll, X.; Basagaña, X.; Dalmau-Bueno, A.; Martinez, D.; Ambros, A.; Cirach, M.; Triguero-Mas, M.; Gascon, M.; Borrell, C.; et al. Green spaces and general health: Roles of mental health status, social support, and physical activity. *Environ. Int.* **2016**, *91*, 161–167. [CrossRef] [PubMed]
5. Parris, K. *Ecology of Urban Environments*; Wiley-Blackwell: Hoboken, NJ, USA, 2016; 240p.
6. Cui, L.; Shi, J. Urbanization and its environmental effects in Shanghai, China. *Urban Clim.* **2012**, *2*, 1–15. [CrossRef]
7. Kalnay, E.; Cai, M. Impact of urbanization and land-use change on climate. *Nature* **2003**, *423*, 528–531. [CrossRef] [PubMed]
8. Shorabeh, S.N.; Kakroodia, A.A.; Firozjaei, M.K.; Minaeia, F.; Homaee, M. Impact assessment modeling of climatic conditions on spatial-temporal changes in surface biophysical properties driven by urban physical expansion using satellite images. *Sustain. Cities Soc.* **2022**, *80*, 103757. [CrossRef]
9. Voogt, J.A.; Oke, T.R. Thermal remote sensing of urban climates. *Remote Sens. Environ.* **2003**, *86*, 370–384. [CrossRef]
10. Oke, T.R.; Mills, R.; Christen, A.; Voogt, J.A. *Urban Climates*; Cambridge University Press: Cambridge, UK, 2017; 519p. [CrossRef]
11. Stewart, I.D.; Mills, G. *The Urban Heat Island. A Guidebook*, 1st ed.; Elsevier: Amsterdam, the Netherlands, 2021; 182p. [CrossRef]
12. Butera, F.M. Climatic change and the built environment. *Adv. Build. Energy Res.* **2010**, *4*, 45–75. [CrossRef]
13. Kapsomenakis, J.; Kolokotsa, D.; Nikolaou, T.; Santamouris, M.; Zerefos, S.C. Forty years increase of the air ambient temperature in Greece: The impact on buildings. *Energy Convers. Manag.* **2013**, *74*, 353–365. [CrossRef]
14. Irmak, M.A.; Yilmaz, S.; Dursun, D. Effect of different pavements on human thermal comfort conditions. *Atmósfera* **2017**, *30*, 355–366. [CrossRef]
15. Unger, J. Comparisons of urban and rural bioclimatological conditions in the case of a Central-European city. *Int. J. Biometeorol.* **1999**, *43*, 139–144. [CrossRef]
16. Morris, K.I.; Kwami, A.C.; Kwami Morris, J.; Ooi, M.C.G.; Oozeer, M.Y.; Abakr, Y.A.; Nadzir, M.S.M.; Mohammed, I.Y.; Al-Qrimli, H.F. Impact of urbanization level on the interactions of urban area, the urban climate, and human thermal comfort. *Appl. Geogr.* **2017**, *79*, 50–72. [CrossRef]
17. Givoni, B. Urban design for hot humid regions. *Renew. Energy* **1994**, *5*, 1047–1053. [CrossRef]
18. Lobaccaro, G.; Acero, J.A. Comparative analysis of green actions to improve outdoor thermal comfort inside typical urban street canyons. *Urban Clim.* **2015**, *14*, 251–267. [CrossRef]
19. Yan, H.; Wu, F.; Dong, L. Influence of a large urban park on the local urban thermal environment. *Sci. Total Environ.* **2018**, *622–623*, 882–891. [CrossRef]
20. Teixeira, C.F.B. Green space configuration and its impact on human behavior and urban environments. *Urban Clim.* **2021**, *35*, 100746. [CrossRef]
21. Vieira, J.; Matos, P.; Mexia, T.; Silva, P.; Lopes, N.; Freitas, C.; Correia, O.; Santos-Reis, M.; Branquinho, C.; Pinho, P. Green spaces are not all the same for the provision of air purification and climate regulation services: The case of urban parks. *Environ. Res.* **2018**, *160*, 306–313. [CrossRef] [PubMed]
22. Hondula, D.M.; Davis, R.E.; Leisten, M.J.; Saha, M.V.; Veazey, L.M.; Wegner, C.R. Fine-scale spatial variability of heat-related mortality in Philadelphia County, USA, from 1983–2008: A case-series analysis. *Environ. Health A Glob. Access Sci. Source* **2012**, *11*, 16. [CrossRef]
23. Ingole, V.; Marí-Dell'Olmo, M.; Deluca, A.; Quijal, M.; Borrell, C.; Rodríguez-Sanz, M.; Achebak, H.; Lauwaet, D.; Gilabert, J.; Murage, P.; et al. Spatial Variability of Heat-Related Mortality in Barcelona from 1992–2015: A Case Crossover Study Design. *Int. J. Environ. Res. Public Health* **2020**, *17*, 2553. [CrossRef]
24. Fenner, D.; Holtmann, A.; Meier, F.; Langer, I.; Scherer, D. Contrasting changes of urban heat island intensity during hot weather episodes. *Environ. Res. Lett.* **2019**, *14*, 124013. [CrossRef]
25. Estoque, R.C.; Murayama, Y. Monitoring surface urban heat island formation in a tropical mountain city using Landsat data (1987–2015). *ISPRS J. Photogramm. Remote Sens.* **2007**, *133*, 18–29. [CrossRef]
26. Meehl, G.A.; Tebaldi, C. More intense, more frequent, and longer lasting heat waves in the 21st Century. *Science* **2004**, *305*, 994–997. [CrossRef]
27. Zhou, B.; Rybski, D.; Kropp, J.P. The role of city size and urban form in the surface urban heat island. *Sci. Rep.* **2017**, *7*, 4791. [CrossRef] [PubMed]
28. Leal Filho, W.; Wolf, F.; Castro-Díaz, R.; Li, C.; Ojeh, V.N.; Gutiérrez, N.; Nagy, G.J.; Savić, S.; Natenzon, C.E.; Quasem Al-Amin, A.; et al. Addressing the Urban Heat Islands Effect: A Cross-Country Assessment of the Role of Green Infrastructure. *Sustainability* **2021**, *13*, 753. [CrossRef]

29. Runnalls, K.E.; Oke, T.R. Dynamics and controls of the near-surface heat island of Vancouver, BC. *Phys. Geogr.* **2000**, *21*, 283–304. [CrossRef]

30. Imhoff, M.L.; Yhang, P.; Wolfe, R.E.; Bounoua, L. Remote sensing of the urban heat island effect across biomes in the continental USA. *Remote Sens. Environ.* **2010**, *114*, 504–513. [CrossRef]

31. Hardin, A.W.; Liu, Y.; Cao, G.; Vanos, J.K. Urban heat island intensity and spatial variability by synoptic weather type in the northeast U.S. *Urban Clim.* **2018**, *24*, 747–762. [CrossRef]

32. Kim, S.W.; Brown, R.D. Urban heat island (UHI) intensity and magnitude estimations: A systematic literature review. *Sci. Total Environ.* **2021**, *779*, 146389. [CrossRef]

33. Oke, T.R. City size and the urban heat island. *Atmos. Environ.* **1973**, *7*, 769–779. [CrossRef]

34. Ramakreshnan, L.; Aghamohammadi, N.; Fong, C.S.; Ghaffarianhoseini, A.; Wong, L.P.; Sulaiman, N.M. Empirical study on temporal variations of canopy-level Urban Heat Island effect in the tropical city of Greater Kuala Lumpur. *Sustain. Cities Soc.* **2019**, *44*, 748–762. [CrossRef]

35. Zou, Z.; Yan, C.; Yu, L.; Jiang, X.; Ding, J.; Qin, L.; Wang, B.; Qiu, G. Impacts of land use/land cover types on interactions between urban heat island effects and heat waves. *Build. Environ.* **2021**, *204*, 108138. [CrossRef]

36. Rajkovich, N.B.; Larsen, L. A Bicycle-Based Field Measurement System for the Study of Thermal Exposure in Cuyahoga County, Ohio, USA. *Int. J. Environ. Res. Public Health* **2016**, *13*, 159. [CrossRef]

37. Schwarz, N.; Lautenbach, S.; Seppelt, R. Exploring indicators for quantifying surface urban heat islands of European cities with MODIS land surface temperatures. *Remote Sens. Environ.* **2011**, *115*, 3175–3186. [CrossRef]

38. Zhou, D.; Zhao, S.; Liu, S.; Zhang, L.; Zhu, C. Surface urban heat island in China's 32 major cities: Spatial patterns and drivers. *Remote Sens. Environ.* **2014**, *152*, 51–61. [CrossRef]

39. Liu, K.; Su, H.; Zhang, L.; Yang, H.; Zhang, R.; Li, X. Analysis of the Urban Heat Island Effect in Shijiazhuang, China Using Satellite and Airborne Data. *Remote Sens.* **2015**, *7*, 4804–4833. [CrossRef]

40. Almeida, C.R.d.; Teodoro, A.C.; Gonçalves, A. Study of the Urban Heat Island (UHI) Using Remote Sensing Data/Techniques: A Systematic Review. *Environments* **2021**, *8*, 105. [CrossRef]

41. Marando, F.; Salvatori, E.; Sebastiani, A.; Fusaro, L.; Manes, F. Regulating Ecosystem Services and Green Infrastructure: Assessment of Urban Heat Island effect mitigation in the municipality of Rome, Italy. *Ecol. Model.* **2019**, *392*, 92–102. [CrossRef]

42. EPA (US Environmental Protection Agency). *Reducing Urban Heat Islands: Compendium of Strategies*; US Environmental Protection Agency: Washington, DC, USA, 2008; 19p.

43. Kim, S.W.; Brown, R.D. Urban heat island (UHI) variations within a city boundary: A systematic literature review. *Renew. Sustain. Energy Rev.* **2021**, *148*, 111256. [CrossRef]

44. Xu, L.Y.; Xie, X.D.; Li, S. Correlation analysis of the urban heat island effect and the spatial and temporal distribution of atmospheric particulates using TM images in Beijing. *Environ. Pollut.* **2013**, *178*, 102–114. [CrossRef] [PubMed]

45. Arnfield, A.J. Two decades of urban climate research: A review of turbulence, exchanges of energy and water, and the urban heat island. *Int. J. Clim.* **2003**, *23*, 1–26. [CrossRef]

46. Zhou, W.; Huang, G.; Cadenasso, M.L. Does spatial configuration matter? Understanding the effects of land cover pattern on land surface temperature in urban landscapes. *Landsc. Urban Plan.* **2011**, *102*, 54–63. [CrossRef]

47. Tzavali, A.; Paravantis, J.; Mihalakakou, G.; Fotiadi, A.; Stigka, E. Urban heat island intensity: A literature review. *Fresenius Environ. Bull.* **2015**, *24*, 4537–4554.

48. Li, Y.; Zhang, X.; Zhu, S.; Wang, X.; Lu, Y.; Du, S.; Shi, X. Transformation of Urban Surfaces and Heat Islands in Nanjing during 1984–2018. *Sustainability* **2020**, *12*, 6521. [CrossRef]

49. Keeratikasikorn, C.; Bonafoni, S. Urban Heat Island Analysis over the Land Use Zoning Plan of Bangkok by Means of Landsat 8 Imagery. *Remote Sens.* **2018**, *10*, 440. [CrossRef]

50. Yu, Z.; Yao, Y.; Yang, G.; Wang, X.; Vejre, H. Spatiotemporal patterns and characteristics of remotely sensed region heat islands during the rapid urbanization (1995–2015) of Southern China. *Sci. Total Environ.* **2019**, *674*, 242–254. [CrossRef]

51. Sun, Y.; Gao, C.; Li, J.; Wang, R.; Liu, J. Evaluating urban heat island intensity and its associated determinants of towns and cities continuum in the Yangtze River Delta Urban Agglomerations. *Sustain. Cities Soc.* **2019**, *50*, 101659. [CrossRef]

52. Zhang, X.; Chen, L.; Jianf, W.; Jin, X. Urban heat island of Yangtze River Delta urban agglomeration in China: Multi-time scale characteristics and influencing factors. *Urban Clim.* **2022**, *43*, 101180. [CrossRef]

53. Busato, F.; Lazzarin, R.M.; Noro, M. Three years of study of the Urban Heat Island in Padua: Experimental results. *Sustain. Cities Soc.* **2014**, *10*, 251–258. [CrossRef]

54. Blachowski, J.; Hajnrych, M. Assessing the Cooling Effect of Four Urban Parks of Different Sizes in a Temperate Continental Climate Zone: Wroclaw (Poland). *Forests* **2021**, *12*, 1136. [CrossRef]

55. Song, J.; Du, S.; Feng, X.; Guo, L. The relationships between landscape compositions and land surface temperature: Quantifying their resolution sensitivity with spatial regression models. *Landsc. Urban Plan.* **2014**, *123*, 145–157. [CrossRef]

56. Bokaie, M.; Shamsipour, A.; Khatibi, P.; Hosseini, A. Seasonal monitoring of urban heat island using multi-temporal Landsat and MODIS images in Tehran. *Int. J. Urban Sci.* **2019**, *23*, 269–285. [CrossRef]

57. Amir Siddique, M.; Wang, Y.; Xu, N.; Ullah, N.; Zeng, P. The Spatiotemporal Implications of Urbanization for Urban Heat Islands in Beijing: A Predictive Approach Based on CA–Markov Modeling (2004–2050). *Remote Sens.* **2021**, *13*, 4697. [CrossRef]

58. Peng, J.; Liu, Q.; Xu, Z.; Lyu, D.; Du, Y.; Qiao, P.; Wu, J. How to effectively mitigate urban heat island effect? A perspective of waterbody patch size threshold. *Landsc. Urban Plan.* **2020**, *202*, 103873. [CrossRef]

59. Athukorala, D.; Murayama, Y. 2021: Urban Heat Island Formation in Greater Cairo: Spatio-Temporal Analysis of Daytime and Nighttime Land Surface Temperatures along the Urban–Rural Gradient. *Remote Sens.* **2021**, *13*, 1396. [CrossRef]

60. Li, X.; Zhou, W.; Ouyang, Z.; Xu, W.; Zheng, H. Spatial pattern of greenspace affects land surface temperature: Evidence from the heavily urbanized Beijing metropolitan area, China. *Landsc. Ecol.* **2012**, *27*, 887–898. [CrossRef]

61. Onishi, A.; Cao, X.; Ito, T.; Shi, F.; Imura, H. Evaluating the potential for urban heat-island mitigation by greening parking lots. *Urban For. Urban Green.* **2010**, *9*, 323–332. [CrossRef]

62. Zhang, Y.; Balzter, H.; Li, Y. Influence of Impervious Surface Area and Fractional Vegetation Cover on Seasonal Urban Surface Heating/Cooling Rates. *Remote Sens.* **2021**, *13*, 1263. [CrossRef]

63. O'Malley, C.; Piroozfar, P.; Farr, E.R.P.; Pomponi, F. Urban Heat Island (UHI) mitigating strategies: A case-based comparative analysis. *Sustain. Cities Soc.* **2015**, *19*, 222–235. [CrossRef]

64. Grilo, F.; Pinho, P.; Aleixo, C.; Catita, C.; Silva, P.; Lopes, N.; Freitas, C.; Santos-Reis, M.; McPhearson, T.; Branquinho, C. Using green to cool the grey: Modelling the cooling effect of green spaces with a high spatial resolution. *Sci. Total Environ.* **2020**, *724*, 138182. [CrossRef]

65. Dimoudi, A.; Nikolopoulou, M. Vegetation in the urban environment: Microclimatic analysis and benefits. *Energy Build.* **2003**, *35*, 69–76. [CrossRef]

66. Pauleit, S.; Hansen, R.; Rall, E.L.; Zölch, T.; Andersson, E.; Luz, A.C.; Szaraz, L.; Tosics, I.; Vierikko, K. *Urban Landscapes and Green Infrastructure*; Oxford University Press: Oxford, UK, 2017; 53p. [CrossRef]

67. Aram, F.; Garcia, E.H.; Solgi, E.; Mansournia, S. Urban green space cooling effect in cities. Review Article. *Heliyon* **2019**, *5*, e01339. [CrossRef]

68. Feyisa, G.L.; Dons, K.; Meilby, H. Efficiency of parks in mitigating urban heat island effect: An example from Addis Ababa. *Landsc. Urban Plan.* **2014**, *123*, 87–95. [CrossRef]

69. Shashua-Bar, L.; Pearlmutter, D.; Erell, E. The cooling efficiency of urban landscape strategies in a hot dry climate. *Landsc. Urban Plan.* **2009**, *92*, 179–186. [CrossRef]

70. Cao, X.; Onishi, A.; Chen, J.; Imura, H. Quantifying the cool island intensity of urban parks using ASTER and IKONOS data. *Landsc. Urban Plan.* **2010**, *96*, 224–231. [CrossRef]

71. Derkzen, M.L.; van Teeffelen, A.J.A.; Verburg, P.H. Quantifying urban ecosystem services based on highresolution data of urban green space: An assessment for Rotterdam, the Netherlands. *J. Appl. Ecol.* **2015**, *52*, 1020–1032. [CrossRef]

72. Pinho, P.; Correia, O.; Lecoq, M.; Munzi, S.; Vasconcelos, S.; Gonçalves, P.; Rebelo, R.; Antunes, C.; Silva, P.; Freitas, C.; et al. Evaluating green infrastructure in urban environments using a multi-taxa and functional diversity approach. *Environ. Res.* **2016**, *147*, 601–610. [CrossRef]

73. Villalobos-Jiménez, G.; Dunn, A.; Hassall, C. Dragonflies and damselflies (Odonata) in urban ecosystems: A review. *Eur. J. Entomol.* **2016**, *113*, 217–232. [CrossRef]

74. Langemeyer, J. *Urban Ecosystem Services. The Value of Green Spaces in Cities*; Stockholm University: Stockholm, Sweden, 2015; 246p.

75. Mexia, T.; Vieira, J.; Príncipe, A.; Anjos, A.; Silva, P.; Lopes, N.; Freitas, C.; Santos-Reis, M.; Correia, O.; Branquinho, C.; et al. Ecosystem services: Urban parks under a magnifying glass. *Environ. Res.* **2018**, *160*, 469–478. [CrossRef]

76. Costanza, R.; D'Arge, R.; de Groot, R.S.; Farber, S.; Grasso, M.; Hannon, B.; Limburg, K.; Naeem, S.; O'Neill, R.V.; Paruelo, J.; et al. The value of world's ecosystem services and natural capital. *Nature* **1997**, *387*, 253–260. [CrossRef]

77. Daily, G.C. (Ed.) *Nature's Services Societal Dependence On Natural Ecosystems*; Island Press: Washington, DC, USA, 1997; 392p.

78. Millennium Ecosystem Assessment. *Ecosystems and Human Well-Being–Synthesis*; Island Press: Washington, DC, USA, 2005; Available online: https://millenniumassessment.org/en/index.html (accessed on 20 June 2022).

79. Park, J.; Kim, J.-H.; Lee, D.K.; Park, C.Y.; Jeong, S.G. The influence of small green space type and structure at the street level on urban heat island mitigation. *Urban For. Urban Green.* **2017**, *21*, 203–212. [CrossRef]

80. Rakoto, P.Y.; Deilami, K.; Hurley, J.; Amati, M.; Sun, Q.C. Revisiting the cooling effects of urban greening: Planning implications of vegetation types and spatial configuration. *Urban For. Urban Green.* **2021**, *64*, 127266. [CrossRef]

81. Zhou, W.; Cao, F.; Wang, G. Effects of Spatial Pattern of Forest Vegetation on Urban Cooling in a Compact Megacity. *Forests* **2019**, *10*, 282. [CrossRef]

82. Su, Y.; Wu, J.; Zhang, C.; Wu, X.; Li, Q.; Bi, C.; Zhang, H.; Lafortezza, R.; Chen, X. Estimating the cooling effect magnitude of urban vegetation in different climate zones using multi-source remote sensing. *Urban Clim.* **2022**, *43*, 101155. [CrossRef]

83. World Health Organization; Regional Office for Europe. *Health and Climate Change: The "Now and How": A Policy Action Guide*; World Health Organization; Regional Office for Europe: Geneva, Switzerland, 2005; 32p. Available online: https://apps.who.int/iris/handle/10665/347913 (accessed on 20 June 2022).

84. ZBGIS® 2021. Basic Database for the Geographic Information System. Geodetic and Cartographic Institute Bratislava (GKÚ) Slovakia. Available online: https://zbgis.skgeodesy.sk/mkzbgis/sk/zakladna-mapa?pos=48.800000,19.530000,8 (accessed on 5 April 2022).

85. Corine Land Cover 2018. Copernicus Land Monitoring Service. Available online: https://land.copernicus.eu/pan-european/corine-land-cover/clc2018?tab=download (accessed on 5 April 2022).

86. Derdouri, A.; Wang, R.; Murayama, Y.; Osaragi, T. Understanding the Links between LULC Changes and SUHI in Cities: Insights from Two-Decadal Studies (2001–2020). *Remote Sens.* **2021**, *13*, 3654. [CrossRef]

87. Klok, L.; Zwart, S.; Verhagen, H.; Mauri, E. The surface heat island of Rotterdam and its relationship with urban surface characteristics. *Resour. Conserv. Recycl.* **2012**, *64*, 23–29. [CrossRef]

88. United States Geological Survey (USGS) EarthExplorer. Available online: https://earthexplorer.usgs.gov/ (accessed on 6 April 2022).

89. Landsat Satellite Missions. United States Geological Survey. Available online: https://www.usgs.gov/landsat-missions/landsat-satellite-missions (accessed on 6 April 2022).

90. Orthophotomosaic. Geodetic and Cartographic Institute Bratislava (GKÚ) Slovakia, National Forest Centre (NLC) Slovakia. Available online: https://www.geoportal.sk (accessed on 5 April 2022).

91. Imperviousness Density, Copernicus Land Monitoring Service. Available online: https://land.copernicus.eu/pan-european/high-resolution-layers/imperviousness/status-maps (accessed on 6 April 2022).

92. ESRI®. Available online: https://www.esri.com (accessed on 4 April 2022).

93. R Core Team. *R: A Language and Environment for Statistical Computing*; R Foundation for Statistical Computing: Vienna, Austria, 2020; Available online: https://www.R-project.org/ (accessed on 5 May 2022).

94. Chander, G.; Markham, B. Revised Landsat-5 TM Radiometric Calibration Procedures and Postcalibration Dynamic Ranges. *IEEE Trans. Geosci. Remote Sens.* **2003**, *41*, 2674–2677. [CrossRef]

95. Yuan, F.; Bauer, M.E. Comparison of impervious surface area and normalized difference vegetation index as indicators of surface urban heat island effects in Landsat imagery. *Remote Sens. Environ.* **2007**, *106*, 375–386. [CrossRef]

96. Carlson, T.N.; Ripley, D.A. On the relation between NDVI, fractional vegetation cover, and leaf area index. *Remote Sens. Environ.* **1997**, *62*, 241–252. [CrossRef]

97. Sobrino, J.A.; Jiménez-Muñoz, J.C.; Paolini, L. 2004: Land surface temperature retrieval from LANDSAT TM 5. *Remote Sens. Environ.* **2004**, *90*, 434–440. [CrossRef]

98. Barsi, J.A.; Schott, J.R.; Palluconi, F.D.; Hook, S.J. Validation of a web-based atmospheric correction tool for single thermal band instruments. *Proc. SPIE* **2005**, *5882*, 58820E.

99. Lepš, J.; Šmilauer, P. *Biostatistics with R: An Introductory Guide for Field Biologists*, 1st ed.; Cambridge University Press: Cambridge, UK, 2020; 382p.

100. Zar, J.H. *Biostatistical Analysis*, 5th ed.; Prentice-Hall/Pearson: Upper Saddle River, NJ, USA, 2010; 944p.

101. Logan, M. *Biostatistical Design and Analysis Using, R. A Practical Guide*; Wiley-Blackwell: Hoboken, NJ, USA, 2010; 546p.

102. Le, C.T.; Eberly, L.E. *Introductory Biostatistics*, 2nd ed.; Wiley: Hoboken, NJ, USA, 2016; 592p.

103. Yanev, I.; Lachezar, F. Assessment of the land surface temperature dynamics in the city of Sofia using Landsat satellite data. *Aerosp. Res. Bulg.* **2017**, *27*, 45–71. [CrossRef]

104. Jain, S.; Sannigrahi, S.; Sen, S.; Bhatt, S.; Chakraborti, S.; Rahmat, S. Urban heat island intensity and its mitigation strategies in the fastgrowing urban area. *J. Urban Manag.* **2020**, *9*, 54–66. [CrossRef]

105. Ma, Y.; Kuang, Y.; Huang, N. Coupling urbanization analyses for studying urban thermal environment and its interplay with biophysical parameters based on TM/ETM+ imagery. *Int. J. Appl. Earth Obs. Geoinf.* **2010**, *12*, 110–118. [CrossRef]

106. Li, H.; Zhou, Y.; Li, X.; Meng, L.; Wang, X.; Wu, S.; Sodoudi, S. A new method to quantify surface urban heat island intensity. *Sci. Total Environ.* **2008**, *624*, 262–272. [CrossRef] [PubMed]

107. Zhu, W.; Sun, J.; Yang, C.; Liu, M.; Xu, X.; Ji, C. How to Measure the Urban Park Cooling Island? A Perspective of Absolute and Relative Indicators Using Remote Sensing and Buffer Analysis. *Remote Sens.* **2021**, *13*, 3154. [CrossRef]

108. Yan, L.; Jia, W.; Zhao, S. The Cooling Effect of Urban Green Spaces in Metacities: A Case Study of Beijing, China's Capital. *Remote Sens.* **2021**, *13*, 4601. [CrossRef]

109. Coutts, A.M.; Harris, R.J.; Phan, T.; Livesley, S.J.; Williams, N.S.G.; Tapper, N.J. Thermal infrared remote sensing of urban heat: Hotspots, vegetation, and an assessment of techniques for use in urban planning. *Remote Sens. Environ.* **2016**, *186*, 637–651. [CrossRef]

110. Rogan, J.; Ziemer, M.; Martin, D.; Ratick, S.; Cuba, N.; DeLauer, V. The impact of tree cover loss on land surface temperature: A case study of central Massachusetts using Landsat Thematic Mapper thermal data. *Appl. Geogr.* **2013**, *45*, 49–57. [CrossRef]

111. Lin, W.; Yu, T.; Chang, X.; Wu, W.; Zhang, Y. Calculating cooling extents of green parks using remote sensing: Method and test. *Landsc. Urban Plan.* **2015**, *134*, 66–75. [CrossRef]

112. Du, J.; Xiang, X.; Zhao, B.; Zhou, H. Impact of urban expansion on land surface temperature in Fuzhou, China using Landsat imagery. *Sustain. Cities Soc.* **2020**, *61*, 102346. [CrossRef]

113. Lepeška, T. The impact of impervious surfaces on ecohydrology and health in urban ecosystems of Banská Bystrica (Slovakia). *Soil Water Res.* **2016**, *11*, 29–36. [CrossRef]

114. Izakovičová, Z.; Mederly, P.; Petrovič, F. Long-Term Land Use Changes Driven by Urbanisation and Their Environmental Effects (Example of Trnava City, Slovakia). *Sustainability* **2017**, *9*, 1553. [CrossRef]

115. Hellings, A.; Rienow, A. Mapping Land Surface Temperature Developments in Functional Urban Areas across Europe. *Remote Sens.* **2021**, *13*, 2111. [CrossRef]

116. Wang, H.; Li, B.; Yi, T.; Wu, J. Heterogeneous Urban Thermal Contribution of Functional Construction Land Zones: A Case Study in Shenzhen, China. *Remote Sens.* **2022**, *14*, 1851. [CrossRef]

117. Yu, X.; Guo, X.; Wu, Z. Land Surface Temperature Retrieval from Landsat 8 TIRS—Comparison between Radiative Transfer Equation-Based Method, Split Window Algorithm and Single Channel Method. *Remote Sens.* **2014**, *6*, 9829–9852. [CrossRef]
118. García-Santos, V.; Cuxart, J.; Martínez-Villagrasa, D.; Jiménez, M.A.; Simó, G. Comparison of Three Methods for Estimating Land Surface Temperature from Landsat 8-TIRS Sensor Data. *Remote Sens.* **2018**, *10*, 1450. [CrossRef]
119. Jiang, Y.; Lin, W. A Comparative Analysis of Retrieval Algorithms of Land Surface Temperature from Landsat-8 Data: A Case Study of Shanghai, China. *Int. J. Environ. Res. Public Health* **2021**, *18*, 5659. [CrossRef]
120. Li, F.; Jackson, T.J.; Kustas, W.P.; Schmugge, T.J.; French, A.N.; Cosh, M.H.; Bindlish, R. Deriving land surface temperature from Landsat 5 and 7 during SMEX02/SMACEX. *Remote Sens. Environ.* **2004**, *92*, 521–534. [CrossRef]
121. Simó, G.; García-Santos, V.; Jiménez, M.A.; Martínez-Villagrasa, D.; Picos, R.; Caselles, V.; Cuxart, J. Landsat and Local Land Surface Temperatures in a Heterogeneous Terrain Compared to MODIS Values. *Remote Sens.* **2016**, *8*, 849. [CrossRef]
122. Laraby, K.G.; Schott, J.R. Uncertainty estimation method and Landsat 7 global validation for the Landsat surface temperature product. *Remote Sens. Environ.* **2018**, *216*, 472–481. [CrossRef]
123. Yu, K.; Chen, Y.; Wang, D.; Chen, Z.; Gong, A.; Li, J. Study of the Seasonal Effect of Building Shadows on Urban Land Surface Temperatures Based on Remote Sensing Data. *Remote Sens.* **2019**, *11*, 497. [CrossRef]
124. Zhao, W.; Duan, S.-B. Reconstruction of daytime land surface temperatures under cloud-covered conditions using integrated MODIS/Terra land products and MSG geostationary satellite data. *Remote Sens. Environ.* **2020**, *247*, 111931. [CrossRef]
125. Wu, P.; Su, Y.; Duan, S.-B.; Li, X.; Yang, H.; Zeng, C.; Ma, X.; Wu, Y.; Shen, H. A two-step deep learning framework for mapping gapless all-weather land surface temperature using thermal infrared and passive microwave data. *Remote Sens. Environ.* **2020**, *277*, 113070. [CrossRef]